

# Electropolymerization of aniline in phosphonium-based ionic liquids and their application as protective films against corrosion

Sinem Ortabay

Department of Chemistry, Engineering Faculty, Istanbul University, Avcılar Istanbul, Turkey

Correspondence to: S. Ortabay (E-mail: ortabay@istanbul.edu.tr)

**ABSTRACT:** Conductive polyaniline (PANI) films were deposited on mild steel by an electropolymerization technique in the presence of different types of phosphonium-based ionic liquids, including tetrabutylphosphonium bromide, tetraoctylphosphonium bromide, and ethyltributylphosphonium diethylphosphate. The formation of the PANI films was followed by repetitive cyclic voltammetry scans and was confirmed with diffuse reflectance infrared Fourier transform spectroscopy. The morphology, surface roughness parameters, and grain sizes of these coatings were evaluated by atomic force microscopy. The corrosion behavior of the bare and PANI-coated electrodes was investigated by potentiodynamic polarization, open-circuit potential, and electrochemical impedance spectroscopy techniques in a simulated marine environment in 3.5 wt % aqueous NaCl solutions. The quantum chemical parameters of the PANI composite films were also calculated with parametric method 3, a semi-empirical quantum mechanical method. The theoretical conclusions were found to be consistent with the reported experimental data. © 2016 Wiley Periodicals, Inc. *J. Appl. Polym. Sci.* **2016**, *133*, 43923.

**KEYWORDS:** coatings; conducting polymers; electrochemistry; ionic liquids; surfaces and interfaces

Received 30 January 2016; accepted 12 May 2016

DOI: 10.1002/app.43923

## INTRODUCTION

Corrosion is an irreversible natural process that causes serious deformation on the surface of metals, alloys, and composites. Corrosive environments dramatically reduce the service life of these materials if necessary precautions are not taken in the design process. Among the several types of corrosion, the most common forms are uniform,<sup>1</sup> pitting,<sup>2</sup> crevice,<sup>3</sup> galvanic,<sup>4</sup> erosion,<sup>5</sup> intergranular,<sup>6</sup> and environmentally assisted cracking.<sup>7</sup> Because each material has inherent and unique corrosion behavior, various techniques have been developed for effective protection from corrosion; these include anodic protection, cathodic protection,<sup>8</sup> and barrier coatings.<sup>9</sup>

Mild steel (MS), which is the most common form of steel, is widely used as a construction material in many industries because of its excellent mechanical properties and the low cost of its productions. The corrosion of steel is a serious problem that strongly affects both natural and industrial environments. The most economic method for protecting steel against corrosion is its isolation from the negative effects of atmospheric components, such as temperature, humidity, and climatic conditions. For this purpose, the use of inhibitors has become important for corrosion control. Among several inhibitor varieties, organic inhibitors have considerable advantages, such as the formation of a hydrophobic film on the metal surface, the

elimination of corrosion in a wide range of pHs, and effectiveness in smaller quantities. The recent trend is to use polymer-supported agents with multiple bonds in their molecular structure, which mostly contains nitrogen and sulfur atoms.<sup>10–12</sup>

Conducting polymers are a relatively new class of polymeric materials, and they have been investigated extensively over the past 2 decades. They have a wide range of applications, such as use in rechargeable batteries, molecular electronics, electronic displays, solar cells, ion-exchange membranes in fuel cells, diodes, capacitors, chemical sensors, drug-release systems, composites, and biosensors. One of the most important applications of these materials is in the corrosion protection of oxidizable metals against corrosion.<sup>13–19</sup>

Among conducting polymers, polyaniline (PANI) has attracted much interest because of the simplicity of its synthesis, its stability at high temperatures, its low production cost, its environmental stability, its nontoxicity, and its high electrical conductivity with variable oxidation levels.<sup>18,19</sup> PANI-containing organic coatings have provided excellent protection from corrosion.<sup>20</sup>

In most coating studies, PANI is doped in alkaline media, neutral solutions, and various types of inorganic acids.<sup>21</sup> For the purposes of corrosion protection, numerous studies have been

**Table I.** Chemical Composition of MS

	C	Si	Mn	P	S	Cr	Mo	Ni	Fe
Composition (%)	0.75	0.15	0.90	0.025	0.025	0.25	0.10	0.40	Balance

performed on PANI composite systems with an aqueous acidic solution, such as PANI–hydrofluoric acid,<sup>22</sup> PANI–benzoate,<sup>21,23,24</sup> PANI/n-TiO<sub>2</sub>,<sup>25</sup> PANI–oxalic acid,<sup>26</sup> or PANI/*p*-toluenesulfonic acid.<sup>27</sup> Recently, the use of ionic liquids (ILs) as polymerization media in several types of polymerization processes has become widespread.<sup>28,29</sup> The low volatility, thermal stability, and high operational potential window make ILs suitable dopant agents for polymeric coatings.<sup>30</sup> It has also been reported that the anionic and cationic species of ILs have a significant influence on the physical and chemical stability of the deposition layer. Thus, factors such as the coating adhesion, uniformity, and corrosion resistance are closely related to the nature of the selected IL.<sup>31</sup> The synthesis of conducting polymers in the presence of ILs also provides significant advantages in the production of different morphologies.<sup>32</sup>

The key objective of this study was to investigate the contribution of phosphonium-based ILs to the corrosion protection efficiency of a PANI coating on the MS surface. In this study, PANI coatings were obtained by cyclic voltammetry (CV) in the presence of three different types of phosphonium-based ILs. The corrosion performances of the conductive PANI-coated electrodes were investigated by potentiodynamic polarization, electrochemical impedance spectroscopy (EIS), and open-circuit potential (OCP) techniques in a 3.5% NaCl solution as a simulated marine environment. The morphological characteristics and the formation of these coatings on the MS surface were elucidated with atomic force microscopy (AFM) and diffuse reflectance infrared Fourier transform (DRIFT) spectroscopy measurements, respectively. The relationship between the molecular structures and corrosion inhibition effect of PANI/IL composites were performed through quantum chemical calculations on the basis of parametric method 3 (PM3). The calculated parameters, including the dipole moment ( $\mu$ ), highest occupied molecular orbital energy ( $E_{\text{HOMO}}$ ), lowest unoccupied molecular orbital energy ( $E_{\text{LUMO}}$ ), gap energy ( $\Delta E$ ), and some structural parameters, could describe the experimental observations well.

## EXPERIMENTAL

### Materials

Aniline (Aldrich), acetonitrile (ACN; Aldrich), tetrabutylphosphonium bromide (TBPB; Sigma-Aldrich), tetraoctylphosphonium bromide (TOPB; Sigma-Aldrich), ethyltributylphosphonium diethylphosphate (ETBPDP; Sigma-Aldrich), NaCl (Merck), ethanol (Merck), and acetone (Merck) chemical reagents were analytical-grade and were used without any further purification. MS specimens, the compositions of which are shown in Table I, cut from the same batch of sheet stock with a 5.0 cm<sup>2</sup> (10.0 × 50.0 × 0.5 mm<sup>2</sup>) area, were used as a substrate material for the purposes of this study. Before each experiment, the surface of the MS electrodes were polished with silicon carbide emery paper up to 1500 grade and then degreased ultrasonically with a 1:1 mix-

ture of acetone and ethanol for a duration of 15 min. The specimens were then rinsed with ACN and dried in a nitrogen atmosphere. After they were dried, the specimens were placed in a desiccator and then used for the experiment.

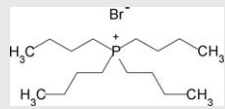
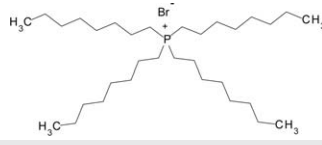
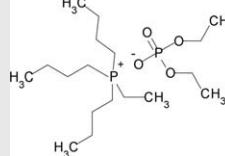
Three different types of phosphonium-based ILs, the cations of which were in quaternary structures, were used as the supporting electrolytes in the electropolymerization experiments. Table II shows the molecular structures of the phosphonium-based ILs.

The electropolymerization of PANI on the MS substrate was studied with the electrochemical CV in an ACN solution containing 0.01 M IL. A three-electrode system was used, and a 1 cm<sup>2</sup> area of the MS sample was exposed to the electrolyte solution as a working electrode. A saturated Ag/AgCl and a platinum electrode served as a reference and counter electrode, respectively, in the electrochemical cell. The CV experiments were maintained with a Gamry Reference 600 potentiostat/galvanostat electrochemical system. The successive cycles, with potentials between −2.0 and 1.0 V, were used for the growth of PANI on the MS surface, and a scan scan rate of 0.050 V/s was applied.

The deposition of PANI was performed in a sequence of 10 cycles after an initial cyclic scan (Figure 1). All of the electropolymerization studies were carried out under a nitrogen atmosphere at room temperature (25 ± 1 °C).

DRIFT analysis was conducted with a Bruker Alpha DRIFT spectrometer with A 528/D model diffuse reflection unit. This included two sample cups. The cup (3 mm deep, 6 mm in diameter) accommodated powdery samples mixed with oven-dried, spectroscopic-grade KBr with a refractive index of 1.559 with an agate mortar and pestle and a 2% concentration. We recorded all of the spectra by averaging 100 scans at a resolution of

**Table II.** Phosphonium-Based ILs Used as Supporting Electrolytes in the Electropolymerization Experiments

IL	Structural formula	Molar mass (g/mol)
TBPB		339.33
TOPB		563.76
ETBPDP		384.47

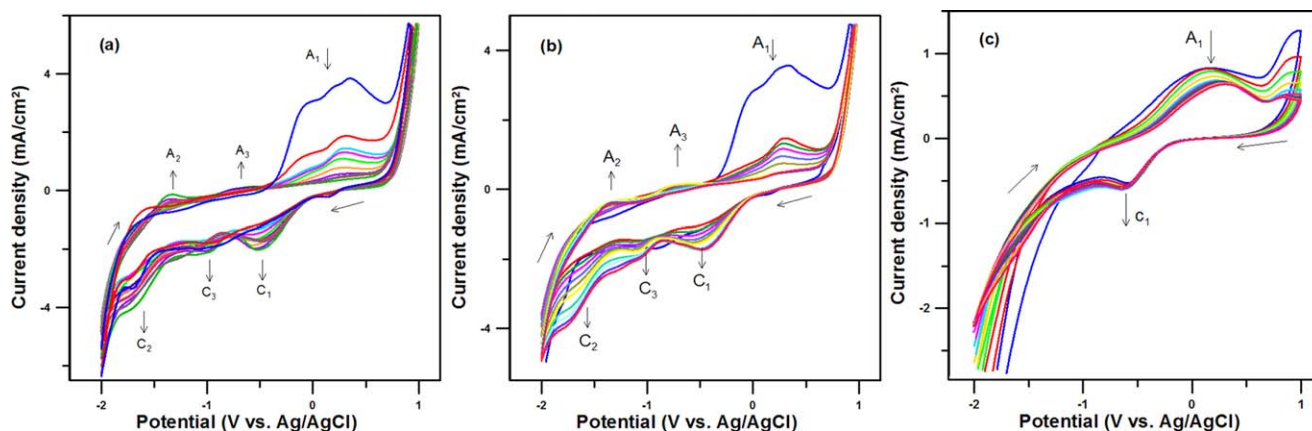


**Figure 1.** CV voltammograms of MS electrodes in the presence of an aniline monomer with an ACN solution containing the following: (a) 0.01 M TBPB, (b) 0.01 M TOPB, or (c) 0.01 M ETBPDP IL medium (scan rate = 0.1 V/s). Arrows show the shift trends of peak currents. [Color figure can be viewed in the online issue, which is available at [wileyonlinelibrary.com](http://wileyonlinelibrary.com).]

$4 \text{ cm}^{-1}$ . Background KBr spectra were obtained, and the spectra of the samples corrected against the background. The spectra were corrected for the effects of atmospheric  $\text{CO}_2$  and humidity and analyzed with OPUS 6.5 software (Bruker Optics, Inc.). The corrosion protection performance of these coatings was investigated in an aqueous 3.5% NaCl solution, which was prepared with ultrapure water with a potentiodynamic polarization technique, EIS, and OCP measurements. These measurements were carried out on an Ivium Vertex potentiostat/galvanostat, the potential control range of which was  $\pm 10 \text{ V}$  and the current range of which was  $\pm 100 \text{ mA}$ . The experiments were performed with a corrosion cell with Ag/AgCl electrodes (saturated KCl) as the reference and Pt wire as the counter electrode. The OCP experiments of the samples were measured versus time for 3 h in aqueous 3.5% NaCl solution. We achieved the potentiodynamic polarization measurements by sweeping the potential between  $-1.5$  and  $0.5 \text{ V}$  from the OCP at a scan rate of  $0.05 \text{ V/s}$ . The EIS measurements were obtained at a corrosion potential ( $E_{\text{corr}}$ ) with the alternating-current amplitude of  $10 \text{ mV}$  for the frequency range of  $10 \text{ mHz}$  to  $100 \text{ kHz}$ . The linear Tafel parts of the anodic and cathodic curves were extrapolated to  $E_{\text{corr}}$  to obtain the corrosion current values. The nanostructural properties and height asymmetries of the resulting films were examined with an AFM instrument, which was produced by Nanomagnetics Instruments. It was operated in dynamic mode at room temperature with aluminum-coated silicon probes (PPP-NCLR nanosensors). The samples were scanned at a  $5 \mu\text{m/s}$  scanning rate and a  $256 \times 256$  pixel resolution to obtain a view with a  $5 \times 5 \mu\text{m}^2$  area. The statistical parameters were calculated from the AFM images with the built-in NMI Viewer 2.0.7 Image Analyser Software. The quantum chemical calculations were performed with the HyperChem 8.0 Professional three-dimensional (3D) molecular modeling program. PM3, a semi-empirical method, was used to obtain the optimized geometries.

## RESULTS AND DISCUSSION

### Electrochemical Deposition of PANI

The MS electrodes were polarized in an ACN solution containing  $0.01 \text{ M}$  phosphonium-based ILs (without aniline monomer) by CV at an electrode potential between  $-2.0$  and  $1.0 \text{ V}$  at a

scan rate of  $0.05 \text{ V/s}$ . The voltammetric responses of the MS electrodes in different supporting electrolytes containing a  $0.01 \text{ M}$  aniline monomer solution are shown in Figure 1(a–c).

The surface barrier effect also increased with repetitive cycles. A well-defined anodic peak, a shoulder, and a cathodic peak appeared at approximately  $0.37 \text{ V}$  [anodic peak 1 (A1)],  $-0.06 \text{ V}$ , and  $-1.69 \text{ V}$  [cathodic peak 1 (C1)], respectively, in the TBPB medium [Figure 1(a)]. The A1 wave and its shoulder obtained in the first step of the electropolymerization process were attributed to the formation of aniline cation radicals. This phenomenon could be explained by the fact that the transformation of leucoemeraldine, which is a fully reduced form of aniline, to its emeraldine form at  $-0.08 \text{ V}$  and the transformation of the emeraldine form to the fully oxidized pernigraniline form at  $0.38 \text{ V}$ .<sup>33</sup> The intensity of A1 gradually decreased, and two new anodic peaks appeared at  $-1.55 \text{ V}$  [anodic peak 2 (A2)] and  $-0.62 \text{ V}$  [anodic peak 3 (A3)], respectively, with consecutive scans. As shown in the figure, the peak current of A2 continued to decrease and almost disappeared at the end of the third scan, but a new peak was observed at  $-1.33 \text{ V}$ . In addition, very small peak currents indicated that an adherent polymer layer was formed on the electrode surface.<sup>34,35</sup> After the first sweep, in the cathodic direction, three reduction waves occurred at  $-0.52 \text{ V}$  (C1),  $-1.00 \text{ V}$  [cathodic peak 3 (C3)], and  $-1.71 \text{ V}$  [cathodic peak 2 (C2)] potentials, and the current values of the peaks increased with the increasing number of scans. This indicated the formation of oligomers and the polymer on the MS surface.<sup>36</sup> A greenish film was observed on the electrode surface after the electrodeposition process, and the obtained electrode was abbreviated as TBPB-MS. The morphology of the film formed on the TBPB-MS surface was homogeneous and compact, and the film strongly adhered to the surface.

As shown in Figure 1(b), similar behavior with TBPB was observed for the electrochemical polymerization of PANI in the TOPB medium. The first cycle showed a large anodic peak at  $0.37 \text{ V}$  (A1), and a shoulder appeared close to  $-0.02 \text{ V}$ . These initial oxidation peaks were assigned to the transformation of leucoemeraldine to pernigraniline step by step via the formation of cation radicals, as mentioned previously.

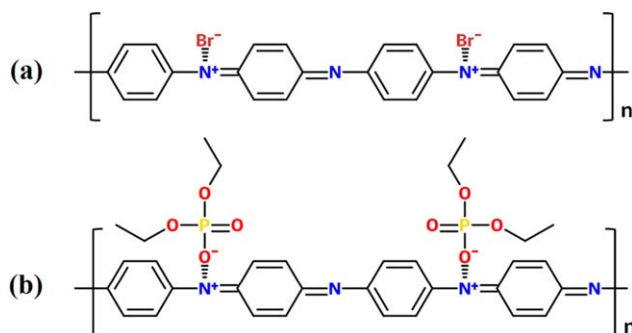
During the repetitive scans, the oxidation potential of pernigraniline (A1) shifted slightly in a negative direction, and the peak current value gradually decreased. This decrease indicated that a hard and homogeneous PANI film layer was formed on the MS surface.<sup>37</sup> However, after the third cycle, two new anodic peaks with relatively weak and broad structures were observed at about  $-1.31$  V (A2) and  $-0.75$  V (A3), whereas the shoulder, located at  $-0.02$  V, completely disappeared. During the reverse sweep, three reduction peaks appeared at about  $-0.47$  V (C1),  $1.08$  V (C3), and  $-1.76$  V (C2), respectively. The current intensities of each reduction wave were found to be greater than that of a previous cycle; this indicated the deposition of an electroactive polymer on the MS surface. A dark green/brownish and quite adhesive PANI coating was observed after the electrochemical process on the MS surface, and the obtained electrode was named TOPB-MS.

Figure 1(c) shows the successive cyclic voltammograms recorded for the polymerization of aniline in an ACN solution containing  $0.01$  M ETBPDP. The first potential scan produced an oxidative wave near  $0.15$  V (A1). After further repetitive cycles within the same range, the peak potentials shifted toward more positive values, and the peak current decreased gradually on the MS surface. On the reverse sweep in the cathodic direction, a reduction peak was observed at about  $-0.21$  V (C1). This indicated a change in the electrode surface at the end of each cycle, as can easily be seen in the figure. These peaks were attributed to the redox conversion of PANI from the conducting emeraldine form to the insulated, nonconducting pernigraniline form because they showed less electroactivity.

We proposed from the CV results that at the initial stage of polymerization, the aniline cation radicals led to the formation of nucleation sites on the electrode surface. This process followed chain-growth polymerization.<sup>38</sup> Because of the viscous nature of IL, negatively charged ions were thought to be adsorbed on the outer surface of the PANI chains.<sup>39</sup>

From the shape of the voltammograms, great similarities were found on the growth and formation of the PANI film for both the TOPB-MS and TBPB-MS electrodes, whereas the ETBPDP-MS differed considerably from them. This condition was attributed to the type of IL used in these experiments. Numerous publications concerning applications of the electropolymerization process in the presence of ILs have demonstrated that ILs have a vigorous effect on the redox reaction of the conductive polymers.<sup>40,41</sup> They are used as components of the polymeric matrices by their direct grafting onto the conjugated polymer chain.<sup>42</sup> The size and the nature of dopant anions of the ILs had a strong influence on the composition of the obtained polymer.<sup>43</sup> From this perspective, it is interesting to note that the ILs containing  $\text{Br}^-$  anion showed more similar electrochemical behavior [Figure 1(a,b)] compared to that containing the diethyl phosphate anion  $[(\text{C}_2\text{H}_5\text{O})_2\text{PO}_2^-]$ ; Figure 1(c)]. The proposed interaction of PANI with the anions of ILs used in the experiment is schematically represented in Figure 2. Similar observations for the formation of polymeric films in the presence of dopant anions were reported earlier.<sup>39</sup>

This behavior could be explained by the fact that the  $\text{Br}^-$  and  $(\text{C}_2\text{H}_5\text{O})_2\text{PO}_2^-$  dopant anions had different sizes and shapes in



**Figure 2.** Proposed chemical structures of the (a) PANI/ $\text{Br}^-$  and (b) PANI/ $(\text{C}_2\text{H}_5\text{O})_2\text{PO}_2^-$  composite systems. [Color figure can be viewed in the online issue, which is available at [wileyonlinelibrary.com](http://wileyonlinelibrary.com).]

the PANI composite system. The ionic radius of the dopant anions had a particular influence on ion transport during the film preparation. A decrease in some of the electrochemical properties, such as the ionic conductivity and charge capacity, occurred as a result of steric hindrance in the polymer matrix because of the impeding ion transport. These effects played an important role in the formation of the surface morphology, especially in the vertical direction.<sup>44</sup> It was also demonstrated that ILs containing phosphonium-based cations provided more stable depositions at the desirable quality.<sup>31</sup>

Among the PANI-coated MS electrodes obtained after the electrochemical polymerization process, ETBPDP-MS was found to have a significantly thicker surface when compared with the others.

#### DRIFT Spectroscopy

DRIFT spectroscopy was used to provide evidence of the polymerization of PANI on the MS surface. The polymeric films were scraped from the electrode surfaces and dispersed in KBr for IR analysis. Figure 3 shows conventional DRIFT spectra obtained from the PANI-coated electrode surfaces.

All of the spectra displayed the characteristic bands of PANI at about  $1620$ ,  $1580$ , and  $1550$   $\text{cm}^{-1}$ ; these bands were assigned to the  $\text{C}=\text{N}$ ,  $\text{C}=\text{C}$  stretching vibrations of quinoid rings, and  $\text{C}-\text{C}$  stretching vibrations of benzenoid rings, respectively.<sup>45</sup> The peaks located at  $1233$  and  $1223$   $\text{cm}^{-1}$  were generated by the  $\text{C}-\text{N}$  stretching vibrations of the secondary ammine groups of the PANI structure.<sup>46</sup> A prominent band was observed in the  $1149$ – $1164$   $\text{cm}^{-1}$  region for all of the samples; this indicated  $\text{C}-\text{H}$  bending vibration modes. The shift toward higher frequencies for three different samples were attributed to the increasing electron delocalization of the benzenoid ring system.<sup>47</sup> For the ETBPDP-MS, this peak was stronger than the others because the internal ethyl group vibrations in the  $\text{P}-\text{O}-\text{C}_2\text{H}_5$  group also contributed to the band located at  $1149$   $\text{cm}^{-1}$ . The region of  $500$ – $1000$   $\text{cm}^{-1}$ , as is well-known, belonged to the aromatic ring and the out-of-plane deformation vibration modes. The most intense peak in this region was observed for the ETBPDP sample. As compared to the other samples, a sharp peak and a prominent shoulder were observed at  $925$  and  $811$   $\text{cm}^{-1}$ , respectively. In addition, the stretching vibrations of the  $\text{P}-\text{O}$  band also contributed to this band.<sup>48</sup>



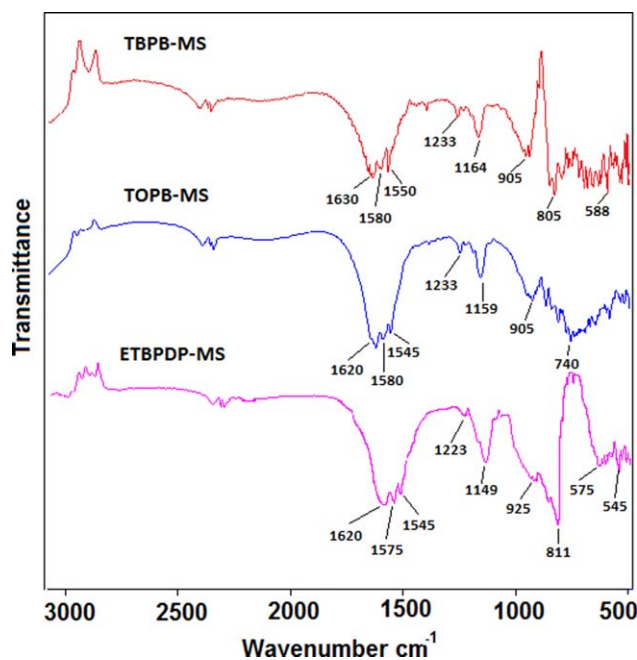


**Figure 3.** DRIFT spectra of the PANI polymeric layers obtained from the TBPB-MS, TOPB-MS, and ETBPDP-MS surfaces. [Color figure can be viewed in the online issue, which is available at [wileyonlinelibrary.com](http://wileyonlinelibrary.com).]

The peak appearing at  $905\text{ cm}^{-1}$  was attributed to the out-of-plane bending of aromatic C–H bonds for TBPB-MS and TOPB-MS.<sup>49</sup> The bands observed at 588, 575, and  $545\text{ cm}^{-1}$  were assigned to the deformation of the quinoid ring. The broad band appearing at  $740\text{ cm}^{-1}$  corresponded to the C–N–C ring bending vibration mode.<sup>50</sup> After the evaluation of all of the results, it was clear that PANI was doped with the anionic parts of the ILs, and this created the PANI/Br and PANI/ $(\text{C}_2\text{H}_5\text{O})_2\text{PO}_2$  structures, as shown in Figure 2. Therefore, it could be said that the IR results showed the characteristic features of doped conductive emeraldine salts, and these results were consistent with the CV experiments.

#### Potentiodynamic Polarization and OCP

Tafel plot analysis was used to study and compare the relative corrosion protection performances of the bare and PANI-coated films synthesized on MS in different ILs medium and were examined in a simulated marine environment in a 3.5% NaCl solution. Figure 4 represents the Tafel plots for the bare MS, PANI-coated TBPB-MS, TOPB-MS, and ETBPDP-MS samples.

As shown in Figure 4, under the same conditions, the PANI films formed in different IL media produced different shifts in  $E_{\text{corr}}$ . The  $E_{\text{corr}}$  values of the PANI-coated MS electrodes shifted in the positive direction compared to that of the bare MS electrode. These results show that MS was better protected when its surface was covered by the PANI film. As shown in the figure, the maximum shift appeared at approximately  $-0.418\text{ V}$  for the ETBPDP-MS electrode, and the minimum shift observed at about  $-0.560\text{ V}$  for TBPB-MS. Table III summarizes the  $E_{\text{corr}}$ , corrosion current density ( $I_{\text{corr}}$ ), and anodic and cathodic Tafel constants ( $\beta_a$  and  $\beta_c$ ), which were determined by extrapolation of the linear portions of the Tafel curves, as shown in Figure 4.

As shown in Table III, the Tafel measurements also clearly revealed that a significant reduction in  $I_{\text{corr}}$  occurred for the PANI-coated MSs with respect to the uncoated MS. This analysis suggested that the PANI coating was strongly adherent and provided almost perfect coverage of the surface.<sup>51</sup> The corrosion protection efficiency (%) values listed in this table were determined from the measured  $I_{\text{corr}}$  values with the following relationship<sup>12</sup>:

$$\text{Protection efficiency (\%)} = \left[ \frac{I_{\text{corr}} - I_{\text{corr(c)}}}{I_{\text{corr}}} \right] \times 100 \quad (1)$$

where  $I_{\text{corr}}$  and  $I_{\text{corr(c)}}$  are the corrosion current values for the bare and PANI-coated MS. The protection efficiencies of the ETBPDP-MS, TOPB-MS, and TBPB-MS were found to be 99.3, 98.3, and 81.2%, respectively. According to these results, the highest protection efficiency against the corrosion of MS was observed for the sample coated with PANI in the ETBPDP solution. This higher corrosion protection efficiency could be attributed to the presence of the  $(\text{C}_2\text{H}_5\text{O})_2\text{PO}_2^-$  dopant anion in the PANI composite structure. In accordance with the previous results, the formation of this structure on MS can provide a more protective layer and prevent an effective electron transfer rate at the interface due to the ionic radius of dopant anion. The results of numerous studies indicate that polymer composites forms with small anions have poorer stability than those with large anions. The reason for this behavior is that smaller doping anions are more likely to be exchanged with external aggressive anions.<sup>52</sup> When viewed from this aspect, the corrosion rates of TBPB-MS and TOPB-MS were expected to be high because they consisted of  $\text{Br}^-$  as a doping anion in the composite matrix. As shown in the table, the TOPB-MS sample was protective enough to completely prevent the corrosion compared to the TBPB-MS. This behavior could be explained

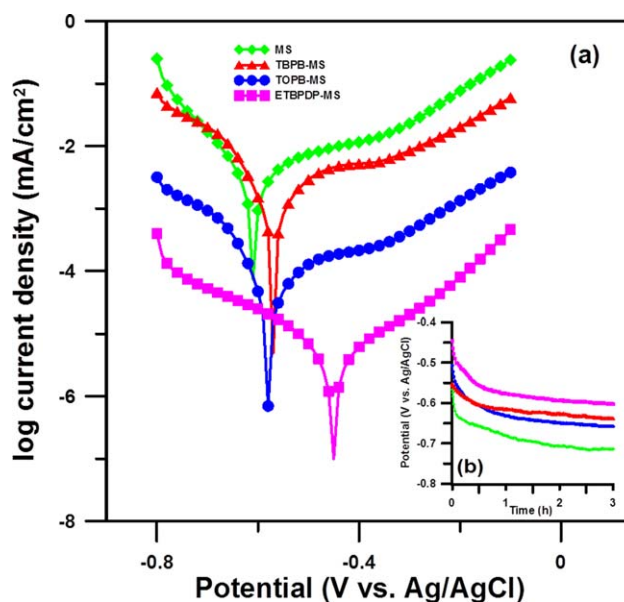


**Figure 4.** Tafel plots of the bare MS, TBPB-MS, TOPB-MS, and ETBPDP-MS recorded in aqueous 3.5% NaCl solutions. The inset shows the variation of OCP with time. [Color figure can be viewed in the online issue, which is available at [wileyonlinelibrary.com](http://wileyonlinelibrary.com).]

**Table III.** Electrochemical Parameters for the Bare MS and PANI-Coated MS in 3.5% NaCl Obtained from Potentiodynamic Polarization Curves

Electrode	$E_{\text{corr}}$ (vs Ag/AgCl)	$i_{\text{corr}}$ (mA/cm <sup>2</sup> )	$\beta_a$ (V/dec)	$\beta_c$ (V/dec)	Corrosion rate (mm/year)	Corrosion protection (%)
MS	-0.612	$4.57 \times 10^{-3}$	0.250	0.114	$5.46 \times 10^1$	—
TBPB-MS	-0.575	$0.86 \times 10^{-3}$	0.343	0.130	$1.85 \times 10^1$	81.2
TOPB-MS	-0.560	$7.58 \times 10^{-5}$	0.260	0.141	$9.04 \times 10^{-1}$	98.3
ETBPDP-MS	-0.418	$6.16 \times 10^{-6}$	0.195	0.280	$7.36 \times 10^{-2}$	99.3

by their cationic group structures. An increase in the alkyl chain length led to an increase in the viscosity of the IL.<sup>53</sup> The lower viscosity of ILs also enhances the polymer chain flexibility because of the ionic mobility. Therefore, these types of structures, which had a high ion mobility in their matrix, were much more prone to corrosion in aggressive media.

The inset of Figure 4 shows the variation of OCP against time in a 3.5 wt % NaCl solution for the PANI/IL coated and uncoated MS samples. At the beginning of the experiment, initial drops in potential were observed for all of the samples. The initial value of OCP for bare MS was found to be -555 mV, and after prolonged immersion in 3.5 wt % NaCl solution, the OCP values shifted toward a more negative potential region and reached an almost constant value of -714 mV after 3 h. This negative shift of OCP was due to the occurrence of general corrosion on the surface of the MS exposed to NaCl solution. The OCP values were found to be 56, 77, and 111 mV more positive for TBPB-MS, TOPB-MS and ETBPDP-MS, respectively, as compared to the that of uncoated MS. The more positive OCP values were due to the effective role of the PANI coatings in the inhibition of the chloride ion diffusion to the MS surface.

### EIS

The corrosion behavior of the bare MS and PANI-coated MS electrodes were further investigated by EIS. The real and imaginary units of the impedance were plotted in Nyquist diagrams. Figure 5 shows the Nyquist plots of the experimental and fitted impedance spectra recorded for the bare MS, TBPB-MS, TOPB-MS, and ETBPDP-MS electrodes at  $E_{\text{corr}}$  in a 3.5% NaCl solution.

The fitting process was performed with the Ivium equivalent circuit evaluator and was optimized with phase, real impedance ( $Z'$ ) and imaginary impedance ( $Z''$ ). The error weight was taken as equal for each point. The equivalent circuit used for the modeling of the impedance spectra is represented by the inset in Figure 5. The simulation of the Nyquist and Bode plots with the following model showed excellent agreement with the experimental data.

$R_s$ ,  $R_{ct}$ , and CPE are the solution resistance, the charge-transfer resistance, and the constant-phase element, respectively. The  $R_{ct}$  values refer to the PANI coating resistance and charge-transfer resistance of the MS/electrolyte interface. CPE is used in the circuit because the electrode/solution interface double layer does not behave as a real capacitor in real corrosion systems. This nonideal capacitance behavior of the coating might have been due to some properties, such as surface roughness or composition, of solid electrodes or the varying thickness of the coated substrate and inhomogeneous reaction rates on the surface.

This kind of behavior of electrodes causes a depressed semicircle in Nyquist plots. Mathematically, the CPE that was comprised of the capacitances of both a double layer and the conductive PANI film in the investigated equivalent circuit model was defined as follows<sup>54</sup>:

$$Z(\text{CPE}) = Y_0^{-1} (j\omega)^{-n} \quad (2)$$

where  $Z(\text{CPE})$  is the impedance of the CPE,  $Y_0$  is the CPE constant,  $j^2 = -1$  is the imaginary unit,  $\omega$  is the angular frequency (rad/s), and  $n$  is the CPE power related to the phase shift. For whole numbers of  $n = 1, 0,$  and  $-1$ , CPE can be expressed as the classical lumped model capacitor, resistance, and inductance, respectively. The value  $n = 0.5$  represents the Warburg impedance. A low  $n$  value means a high surface roughness or heterogeneity of the electrode.<sup>55</sup>

The Nyquist plots for the bare MS and all of the PANI-coated MS were characterized by one depressed semicircular capacitive loop (Figure 5). The shape of the capacitive loops suggested that the charge-transfer process controlled the corrosion of electrodes at  $E_{\text{corr}}$ .<sup>56</sup> On the other hand, the diameter of the depressed semicircle increased gradually in the order MS, TBPB-MS, TOPB-MS, and ETBPDP-MS, respectively. Such behavior is characteristic of solid electrodes and is generally attributed to the surface

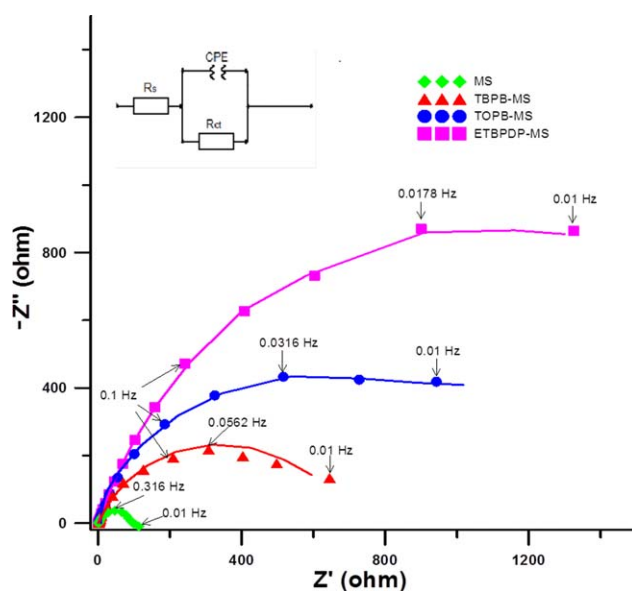


**Figure 5.** Nyquist plots of the bare MS and its PANI-coated substrates in the presence of 3.5% NaCl at  $E_{\text{corr}}$ . The inset shows the equivalent circuit used for modeling the impedance spectra. [Color figure can be viewed in the online issue, which is available at [wileyonlinelibrary.com](http://wileyonlinelibrary.com).]

**Table IV.** EIS Fit Parameters Obtained from the Equivalent Circuit Model for the Bare MS and PANI-Coated MS in 3.5% NaCl Solutions

Electrode	$R_s$ (ohm)	$R_{ct}$ (ohm)	$C_{dl}$ (mF/cm <sup>2</sup> )	$n$	Protection efficiency (%)
MS	1.028 ± 0.002	96.98 ± 0.01	5.193	0.871	—
TBPB-MS	0.695 ± 0.015	680.30 ± 0.09	4.165	0.821	85.74
TOPB-MS	0.758 ± 0.026	1283.00 ± 2.27	3.928	0.802	92.44
ETBPDP-MS	0.997 ± 0.021	2623.00 ± 2.67	3.410	0.792	96.30

heterogeneity due to the inhibitor adsorption and the formation of porous layers on a metal surface.<sup>57</sup>

The electrochemical impedance parameters, including  $R_s$ ,  $R_{ct}$ ,  $C_{dl}$  (double layer capacitance), and  $n$ , obtained from fitting the recorded EIS data with the equivalent circuit, are listed in Table IV. The  $C_{dl}$  values were derived from the CPE parameters according to the following equation<sup>58</sup>:

$$C_{dl} = (Y_0 R_{ct}^{1-n})^{1/n} \quad (3)$$

The protection efficiency was calculated from the  $R_{ct}$  values with eq. 4<sup>58</sup>:

$$\text{Protection efficiency (\%)} = \frac{R'_{ct} - R_{ct}^0}{R'_{ct}} \times 100 \quad (4)$$

where  $R'_{ct}$  and  $R_{ct}^0$  are the charge-transfer resistances of the bare MS and PANI-coated MS samples, respectively.

It is shown clearly in Table IV that the capacitance values gradually decreased from 5.193 to 3.410 mF, whereas the  $R_{ct}$  values ranged from 96.98 to 2623  $\Omega$  for MS, TBPB-MS, TOPB-MS, and ETBPDP-MS, respectively. These phenomena are generally described as the corrosion inhibition of a metal with the formation of a protective layer of adsorbed species on the metal surface. The higher  $R_{ct}$  values of the PANI-coated MS were attributed to the permeation on the electrode surface of corrosive chloride ions; this was inhibited by the PANI polymer coating. The decrease in the local dielectric constant and/or increase in the thickness of the electrical double layer led to a decrease in the capacitance values with the formation of the PANI polymer on the metal surface, in accordance with the following Helmholtz equation<sup>21</sup>:

$$C_{dl} = \frac{\epsilon \epsilon_0 r A}{d} \quad (5)$$

where  $\epsilon$  is the relative dielectric constant of the coated film,  $\epsilon_0$  is the permittivity of the vacuum ( $8.85 \times 10^{-14}$  F/cm),  $d$  is the coating thickness, and  $r$  is the ratio of the effective surface area to the geometric area ( $A$ ).

The  $n$  parameters presented decreasing trends from the bare MS to the ETBPDP-MS electrodes in the range of 0.871 to 0.792. This behavior could be explained by the reduction of the surface homogeneity due to the adsorption of the conducting PANI polymer on the active adsorption sites.<sup>59</sup> From the protection efficiency values, the MS-ETBPDP electrode exhibited the best protection against corrosion from among the other protective coatings. As can be compared with the results in Table III, the protection efficiency values calculated by both potentiody-

namic polarization and electrochemical impedance methods were found to be in good agreement.

The high-frequency range portion of the impedance and phase angle ( $-\alpha^\circ$ ) plots expressed the behavior of a heterogeneous surface layer, whereas the low-frequency (LF) range showed the kinetic response for the charge-transfer reaction. For the Bode-impedance ( $|Z|$ ) plots, the high-frequency impedance corresponded to  $R_s$ , whereas the LF impedance expressed the total impedance.

As shown in Figure 6(a), only one time constant could be distinguished in all of the phase diagrams in the medium-frequency range. These phase diagrams were observed to get higher and broader from MS to ETBPDP-MS electrodes. The  $-\alpha^\circ$  and the slope ( $-S$ ) values obtained from the Bode phase plots in Figure 6(a,b) are presented in Table V. The values of the maximum  $-\alpha^\circ$  ranged from 61.03 and 71.40, whereas the  $-S$  values obtained from the Bode impedance plots changed between  $-0.698$  and  $-0.793$  for the uncoated and PANI-coated electrodes. Such deviations of these parameters from the ideal values of 90 ( $-\alpha^\circ$ ) and  $-1$  ( $-S$ ) also supported the nonideal behavior of capacitance, as mentioned in earlier sections. In the medium-frequency range between about 0.1 and 1000 Hz, a large negative  $-\alpha^\circ$  was observed for the PANI-coated samples. This may also have been indicative of a high corrosion resistance and the large capacitive behavior of the polymer-coated layer.<sup>60</sup> The increasing values of  $|Z|$  confirmed that the PANI inhibited corrosion by forming a protective film on the outer surface layer. Therefore, the corrosion protection efficiency increased in the following order: ETBPDP-MS > TOPB-MS > TBPB-MS.

#### AFM Measurements

AFM is a powerful technique used for characterizing the surface morphology on the nanometer scale. It is possible to evaluate characteristics such as roughness, porosity, average size, and particle size distribution, which directly affect the optical, mechanical, surface, magnetic, and electrical properties of thin films. Therefore, over the last decade, this technique has become a new method for controlling the surface structure of polymer films.<sup>61</sup>

To understand the surface morphology of the electrodes investigated in this study, AFM analyses were performed after the electropolymerization of the PANI onto the MS surface in the presence of the different types of ILs studied. The 3D AFM images, cross-sectional scans, and height distribution histograms of the MS, TBPB-MS, TOPB-MS, and ETBPDP-MS electrodes are shown Figure 7(a-d).

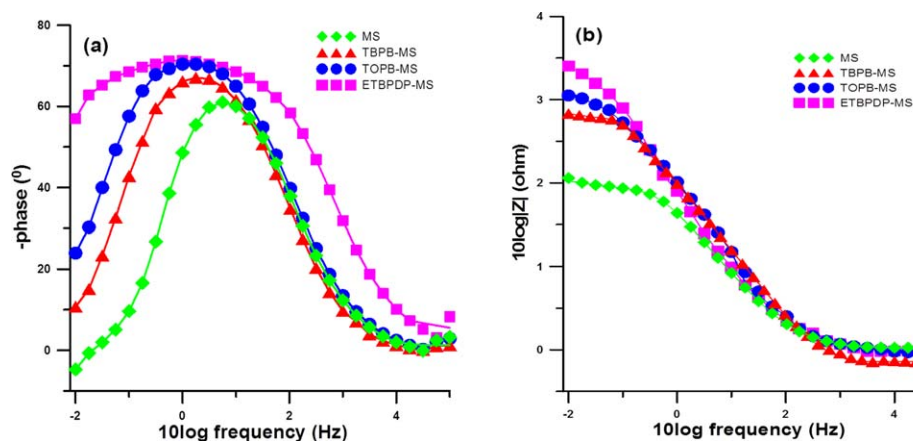


**Figure 6.** (a) Bode phase plots and (b) Bode impedance plots of the MS, TBPB-MS, TOPB-MS, and ETBPDP-MS electrodes in 3.5% NaCl solutions. [Color figure can be viewed in the online issue, which is available at [wileyonlinelibrary.com](http://wileyonlinelibrary.com).]

The average roughness, root mean square (RMS) roughness, surface skewness, and surface kurtosis parameters of the electrodes were determined with the help of the AFM images shown in Figure 7. The obtained results are listed in Table VI. As shown in the AFM images, the surface of the bare MS was fairly uniform with a flat surface, whereas the coated MSs were fully covered by the PANI polymer film. Scratches were clearly visible on the bare MS surface and were caused by the polishing procedure. These polishing scratches yielded an RMS roughness of 56 nm. When compared to the other PANI-coated MS electrodes, the TBPB-MS surface had a more compact and bumpy structure, and the surface roughness of this electrode was approximately 202 nm. For the TOPB-MS electrode, a homogeneously distributed porous and spiky structure was noticed. The depth of these pores was estimated to be approximately 0.05  $\mu\text{m}$  from the cross-sectional analysis given in Figure 7(c). The difference in the surface structures of TBPB-MS and TOPB-MS may have been due to the length of the hydrocarbon chains in the ILs (Table II). Thus, we concluded that the longer hydrocarbon tail of the IL was responsible for enhancing the porosity in the PANI film.<sup>41</sup> As shown in the AFM images of the ETBPDP-MS electrode given in Figure 7(d), islandlike clusters of various scales were distributed in the polymer films. It was clearly observed that the valleys, mountains, and islandlike structures had different irregular sizes and separations and became bigger on the surface when compared with that of the TOPB-MS electrode. This surface structure was found to be in accordance with the results of the EIS method.

As shown in Table VI, the average roughness and RMS roughness values for the bare MS samples were found to be lower than those for the samples of the PANI-coated samples, as expected. The highest surface roughness was obtained for the ETBPDP-MS (average roughness = 257 nm and RMS roughness = 265 nm) among the other electrodes, whereas the smallest value was noted for the bare MS sample (average roughness = 57 nm and RMS roughness = 56 nm). The corresponding values of the TBPB-MS electrode were higher than those of the TOPB-MS. The TBPB-MS surface possessed a deep valley and a high, mountedlike formation in specific regions. This led to an increase in the RMS roughness values, although most of the

parts of this surface had a uniform and flat structure. All of these roughness behaviors were attributed to the selective adsorption occurring during the electropolymerization process of PANI in the presence of different types of ILs.

The AFM images were also used to calculate the height asymmetry and distribution of electrode surfaces. For this purpose, skewness and kurtosis values were determined with the aid of the quantitative surface roughness parameters. The surface kurtosis value is a measurement of the peakness or sharpness of a surface, whereas the skewness parameter signifies the asymmetry of surface heights with respect to the mean surface. The positive skewness parameters revealed that the surfaces had more peaks than valleys, and the kurtosis values were revealed to be smaller than 3. This indicated that the surfaces had a flatter distribution than normal. The surface kurtosis value of 3 indicated a Gaussian amplitude distribution, and the surface possessed an equal number of valleys and peaks.<sup>62</sup> All of the electrodes prepared in this study exhibited positive skewness and kurtosis values of less than 3. From the histogram graphs, we observed that the grain size of the coated MS electrodes became larger for TBPB-MS, TOPB-MS, and ETBPDP-MS, respectively.

#### Quantum Chemical Calculation

Semi-empirical quantum mechanical methods were performed with the HyperChem 8.0 Professional 3D molecular modeling program to investigate the effect of the molecular structure on the inhibition mechanism and the inhibition efficiency. The geometrical optimization of the PANI/ILs was obtained with PM3, which is a semi-empirical method for the quantum

**Table V.** Values of  $-\alpha^\circ$  and  $-S$  of Bode Phase Plots for the Bare MS and PANI-Coated MS Electrodes in 3.5% NaCl Aggressive Solutions

Electrode	$-S$	$-\alpha^\circ$
MS	0.698	61.03
TBPB-MS	0.793	67.06
TOPB-MS	0.716	70.04
ETBPDP-MS	0.749	71.40



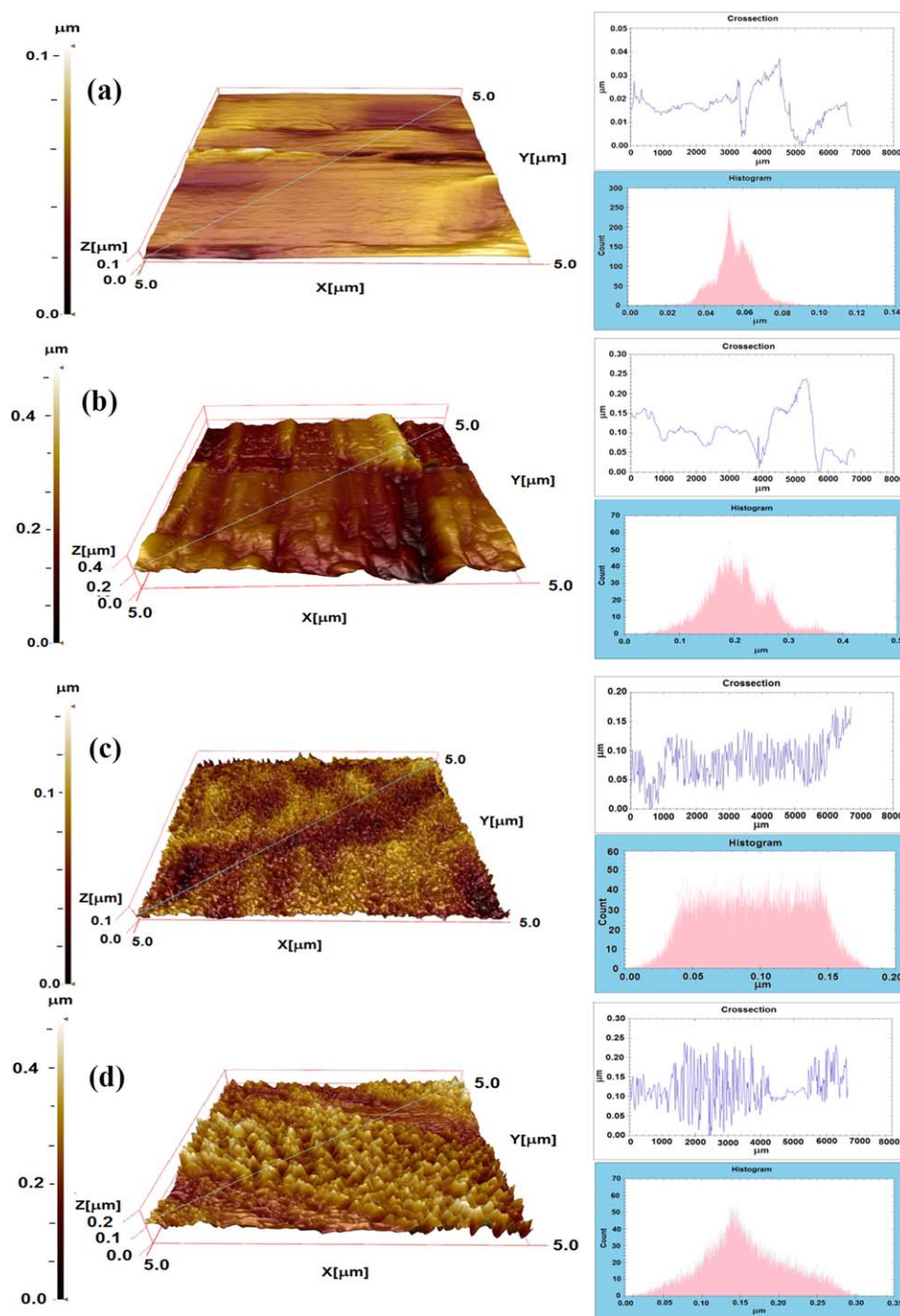


**Figure 7.** AFM surface 3D images, depth profiles, and height distribution histograms of (a) MS, (b) TBPB-MS, (c) TOPB-MS, and (d) ETBPDP-MS electrodes. [Color figure can be viewed in the online issue, which is available at [wileyonlinelibrary.com](http://wileyonlinelibrary.com).]

**Table VI.** Statistical Parameters Obtained from the AFM Images of MS, TBPB-MS, TOPB-MS, and ETBPDP-MS

	Average roughness (nm)	RMS roughness (nm)	Surface skewness	Surface kurtosis
MS	57.0	56.0	1.022	0.06
TBPB-MS	195.0	202.0	1.079	1.221
TOPB-MS	104.0	111.0	1.172	1.497
ETBPDP-MS	257.0	265.0	1.091	1.256

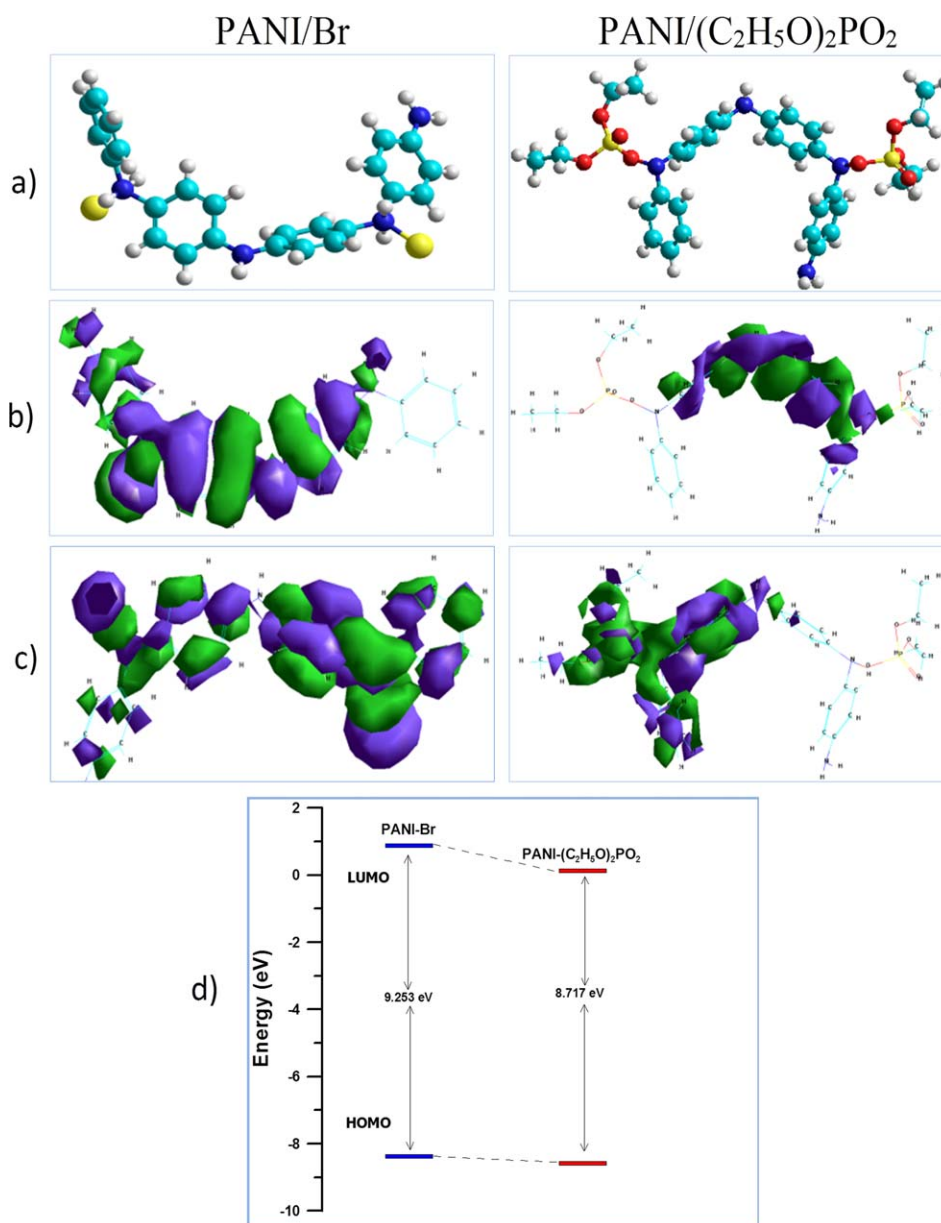


**Figure 8.** (a) Optimized molecular structures, (b) highest occupied molecular orbitals (HOMOs), and (c) lowest unoccupied molecular orbitals (LUMOs) of the PANI/Br<sup>-</sup> and PANI/(C<sub>2</sub>H<sub>5</sub>O)<sub>2</sub>PO<sub>2</sub><sup>-</sup> nanocomposites and (d) schematic diagrams of the energy levels and calculated  $\Delta E$  (eV) values. [Color figure can be viewed in the online issue, which is available at [wileyonlinelibrary.com](http://wileyonlinelibrary.com).]

calculation of the molecular electronic structure in computational chemistry. The quantum parameters, such as  $E_{\text{HOMO}}$ ,  $E_{\text{LUMO}}$ ,  $\Delta E$  ( $E_{\text{LUMO}} - E_{\text{HOMO}}$ ), and  $\mu$ , are strongly related to the inhibition efficiency.<sup>63</sup>

The  $E_{\text{LUMO}}$  parameter signifies the electron-receiving tendency, whereas the  $E_{\text{HOMO}}$  parameter refers to the electron-donating ability of a molecule.<sup>64</sup> The parameter  $\Delta E$  is an important parameter for measuring the overall reactivity of the inhibitor molecule toward the adsorption on the metallic surface. Low values of  $\Delta E$  indicate a higher inhibition efficiency because the energy needed to remove an electron from the last occupied orbital will be minimized. The optimized structures of the studied molecules are shown in Figure 8, and the calculated energies

$E_{\text{HOMO}}$ ,  $E_{\text{LUMO}}$ , and  $\Delta E$  and other parameters are given in Table VII. As shown in the table, it was clear that the values of  $\Delta E$  increased in the order PANI/Br > PANI/(C<sub>2</sub>H<sub>5</sub>O)<sub>2</sub>PO<sub>2</sub>. This suggests that PANI/(C<sub>2</sub>H<sub>5</sub>O)<sub>2</sub>PO<sub>2</sub> had the highest reactivity, and its adsorption on the MS surface due to a strong columbic interaction facilitated the inhibition efficiency compared to that of PANI/Br.

The  $\mu$  value of the molecules was another important factor that needed to be considered.

The higher values of  $\mu$  were responsible for the enhancement of the adsorption capacity between the inhibitor and metal surface, and this explained the highest inhibition efficiency.<sup>65</sup>

**Table VII.** Quantum Chemical Parameters of the Composite Inhibitors

	PANI/Br	PANI/(C <sub>2</sub> H <sub>5</sub> O) <sub>2</sub> PO <sub>2</sub>
Total energy (kcal/mol)	-103,929.0	-176,416.0
$\mu$ (D)	1.772	2.387
Surface area	605.99	949.75
Volume (Å <sup>3</sup> )	1220.80	1862.86
Polarizability (Å <sup>3</sup> )	50.07	65.23
Mass (amu)	524.26	670.64
Highest occupied molecular orbital (eV)	-8.367	-8.589
Lowest unoccupied molecular orbital (eV)	0.886	0.128
$\Delta E$ (eV)	9.253	8.717

To characterize the inhibition activity of the inhibitor molecules, some other parameters, such as molecular volume, molecular surface area, polarizability, and total energy, can be also taken into consideration.

The increasing molecular volume and molecular surface area led to better coverage of the surface and increased the inhibition efficiency. The polarizability is known to be proportional to the induced  $\mu$  value. The increasing polarizability caused the inhibitor molecules to leave the electrolyte and be accumulated by the metallic surface to form a protective thin film. Therefore, the increasing polarizability resulted in a higher inhibition efficiency.<sup>66</sup>

The total energy refers to the sum of the potential and kinetic energies of the inhibitor molecule and gives information about the reactivity and stability of a molecule.<sup>46</sup> A decreasing trend in the total energy is generally attributed to an increasing inhibition efficiency as well. As shown in Table VII, all of the parameters mentioned previously correlated well with the order of the experimental results obtained from the electrochemical studies for the inhibition efficiencies [PANI/(C<sub>2</sub>H<sub>5</sub>O)<sub>2</sub>PO<sub>2</sub> > PANI/Br].

## CONCLUSIONS

In this study, the electrochemical polymerization of PANI films was successfully performed in TBPB, TOPB, and ETBPDP/ACN IL solutions on an MS surface by the use of an electrochemical polymerization technique. The results clearly show that the response of the PANI films was dependent on the type of the electrolyte used in the experiments. A DRIFT spectroscopy study of the PANI-coated samples revealed the presence of both quinoid and benzenoid structures, which were characteristic of the conductive emeraldine salt of PANI. It was also confirmed that the diethyl phosphate group of the anionic part of ETBPDP was incorporated in the polymeric PANI structure. The results of EIS measurements and potentiodynamic polarization studies showed that the synthesized PANI films had considerable corrosion protection efficiency in an aggressive medium of 3.5% NaCl solution. The best corrosion resistance was achieved up to 99.3% for the ETBPDP-MS surface. The AFM studies showed the surface morphology, grain size, and distribution of polymeric formations on the MS surface. In addition, the morphologies of the surfaces were found to be consistent with the

results of the corrosion studies. The results obtained from the quantum chemical calculations of the PANI-Br and PANI/(C<sub>2</sub>H<sub>5</sub>O)<sub>2</sub>PO<sub>2</sub><sup>-</sup> composite systems show that stronger columbic interactions facilitated the inhibition efficiency.

## REFERENCES

- Zhang, X.; Ba, Z.; Wang, Q.; Wu, Y.; Wang, Z.; Wang, Q. *Corros. Sci.* **2014**, *88*, 1.
- Amin, M. A. *Corros. Sci.* **2010**, *52*, 3243.
- Chen, X.; Wang, G.; Gao, F.; Wang, Y.; He, C. *Corros. Sci.* **2015**, *101*, 1.
- Hack, H. P. In Reference Module in Materials Science and Materials Engineering; Elsevier: Amsterdam, **2016**; Vol. 2, p 828.
- Calderón, J. A.; Jiménez, J. P.; Zuleta, A. A. *Surf. Coat. Technol.* DOI: 10.1016/j.surfcoat.2016.04.063.
- Gwinner, B.; Auroy, M.; Balbaud-Célérier, F.; Fauvet, P.; Larabi-Gruet, N.; Laghoutaris, P.; Robin, R. *Corros. Sci.* **2016**, *107*, 60.
- Ilman, M. N. *Int. J. Fatigue* **2014**, *62*, 228.
- Jones, D. A. In Corrosion; Newnes-Butterworths: London, **1976**; Chapter 11, p 13.
- Grgur, B. N.; Elkais, A. R.; Gvozdenović, M. M.; Drmanić, S. Ž.; Trišović, T. L.; Jugović, B. Z. *Prog. Org. Coat.* **2015**, *79*, 17.
- Morales-Gil, P.; Negron-Silvab, G.; Romero-Romo, M.; Angeles-Chavez, C.; Palomar-Pardave, M. *Electrochim. Acta* **2004**, *49*, 4733.
- Roussi, E.; Tsetsekou, A.; Tsiourvas, D.; Karantonis, A. *Surf. Coat. Technol.* **2011**, *205*, 3235.
- Tiu, B. D. B.; Advincula, R. C. *React. Funct. Polym.* **2015**, *95*, 25.
- Bhandari, H.; Kumar, S. A.; Dhawan, S. K. In Nanocomposites—New Trends and Developments; Ebrahimi, F., Ed.; Intech: Rijeka, Croatia, **2012**; Chapter 13, p 329.
- Santos, L. H. E.; Branco, J. S. C.; Guimaraes, I. S.; Motheo, A. *J. Surf. Coat. Technol.* **2015**, *275*, 26.
- Selvakumar, M.; Pitchumani, S. *Korean J. Chem. Eng.* **2010**, *27*, 977.
- Das, T. K.; Prusty, S. *Polym. Plast. Technol. Eng.* **2012**, *51*, 1487.
- De Souza Gomes, A. In New Polymers for Special Applications; Intech: Rijeka, Croatia, **2012**; Chapter 1, p 1.
- Ashassi-Sorkhabi, H.; Es'haghi, M. *J. Mater. Eng. Perform.* **2013**, *22*, 3755.
- Zampetti, E.; Pantalei, S.; Scalese, S.; Bearzotti, A.; De Cesare, F.; Spinella, C.; Macagnano, A. *Biosens. Bioelectron.* **2011**, *26*, 2460.
- Sathiyarayanan, S.; Muthkrishnan, S.; Venkatachari, G. *Electrochim. Acta* **2006**, *51*, 6313.
- Correa, C. M.; Faez, R.; Bizeto, M. A.; Camilo, F. F. *RSC Adv.* **2012**, *2*, 3088.
- Zhang, Y.; Shao, Y.; Zhang, T.; Meng, G.; Wang, F. *Corros. Sci.* **2011**, *53*, 3747.

23. Popović, M. M.; Grgur, B. N. *Synth. Met.* **2004**, *143*, 191.
24. Kamaraj, K.; Sathiyarayanan, S.; Muthukrishnan, S.; Venkatachari, G. *Prog. Org. Coat.* **2009**, *64*, 460.
25. Pagotto, J. F.; Recio, F. J.; Motheo, A. J.; Herrasti, P. *Surf. Coat. Technol.* **2016**, *289*, 23.
26. Camalet, J. L.; Lacroix, J. C.; Aeiyaich, S.; Chane-Ching, K.; Lacaze, P. C. *Synth. Met.* **1998**, *93*, 133.
27. Camalet, J. L.; Lacroix, J. C.; Aeiyaich, S.; Lacaze, P. C. *J. Electroanal. Chem.* **1998**, *445*, 117.
28. Elsentriecy, H. H.; Qu, J.; Luo, H.; Meyer, H. M.; Ma, C.; Chi, M. *Thin Solid Films* **2014**, *568*, 44.
29. Tawde, S.; Mukesh, D.; Yakhmi, J. V. *Synth. Met.* **2002**, *125*, 410.
30. Abbott, A. P.; McKenzie, K. J. *Phys. Chem. Chem. Phys.* **2006**, *8*, 4265.
31. Robert Petro, M. S.; Song, G. L. In *Modern Electroplating*; Schlesinger, M., Paunovic, M., Eds.; Wiley: Hoboken, NJ, **2010**; p 665.
32. Kowsari, E.; Faragh, G. *Ultrason. Sonochem.* **2010**, *17*, 718.
33. Zheng, D.; Hu, C.; Peng, Y.; Hu, S. *Electrochim. Acta* **2009**, *54*, 4910.
34. Sayyah, S. M.; Khaliel, A. B.; Azooz, R. E.; Mohamed, F. In *Electropolymerization*; Schab-Balcerzak, E., Ed.; Intech: Rijeka, Croatia, **2012**; Chapter 2, p 21.
35. Yağan, A.; Özçiçek Pekmez, N.; Yıldız, A. *Corros. Sci.* **2007**, *49*, 2905.
36. Zor, S.; Yakar, E. *Bull. Electrochem.* **2007**, *23*, 149.
37. Lua, J.; Yan, F.; Texter, J. *Prog. Polym. Sci.* **2009**, *34*, 431.
38. Combellas, C.; Delamar, M.; Kanoufi, F.; Pinson, J.; Podvorica, F. I. *Chem. Mater.* **2005**, *17*, 3968.
39. Zhang, J.; Lei, J.; Liu, Y.; Zhao, J.; Ju, H. *Biosens. Bioelectron.* **2009**, *24*, 1858.
40. Handy, S. T. In *Applications of Ionic Liquids in Science and Technology*; Tsubokawa, N., Ed.; Intech: Rijeka, Croatia, **2010**; p 173.
41. Bidan, G. In *Electropolymerization: Concepts, Materials and Applications*; Cosnier, S., Karyakin, A., Eds.; Wiley-VCH: Weinheim, **2010**; Chapter 1, p 1.
42. Mecerreyes, D. In *Ionic Liquids as Polymer Additives*; Livi, S., Gerard, J.-F., Duchet-Rumeau, J., Eds.; Springer: Berlin, **2015**; Chapter 1, p 1.
43. Eftekhari, A.; Kazemzad, M.; Keyanpour-Rad, M. *Polym. J.* **2006**, *38*, 781.
44. Trchova, M.; Stejskal, J. *Pure Appl. Chem.* **2011**, *83*, 1803.
45. Rangel-Vázquez, N. A.; Salgado-Delgado, R.; García-Hernández, E.; Mendoza-Martínez, A. M. *J. Mex. Chem. Soc.* **2009**, *53*, 248.
46. Liu, W.; Yan, X.; Chen, J.; Feng, Y.; Xue, Q. *Nanoscale* **2013**, *5*, 6053.
47. Lin-Vien, D.; Colthup, N. B.; Fateley, W. G.; Graselli, J. G. *The Handbook of Infrared and Raman Characteristic Frequencies of Organic Molecules*, United Kingdom Edition; Academic: London, **1991**; Chapter 16, p 263.
48. Kalsi, P. S. In *Spectroscopy of Organic Compounds*; New Age International: New Delhi, **2007**; Chapter 3, p 65.
49. Silverstein, R. M.; Francis, X. In *Spectrometric Identification of Organic Compounds*; Wiley: Hoboken, NJ, **2014**; Chapter 2, p 71.
50. Shokry, H. *Chem. Met. Alloys* **2009**, *2*, 202.
51. Yi, Y.; Liu, G.; Jin, Z.; Feng, D. *Int. J. Electrochem. Sci.* **2013**, *8*, 3540.
52. Makhoulouf, A. S. H. In *Handbook of Smart Coatings for Materials Protection*; Elsevier: Waltham, MA, **2011**; Part 17, p 469.
53. Yamaguchi, T.; Nakahara, E.; Koda, S. *Jpn. J. Phys. Chem. B* **2014**, *118*, 5752.
54. Singh, A. K.; Mohapatra, S.; Pani, B. *J. Ind. Eng. Chem.* **2016**, *33*, 288.
55. MES 25: *Electrochemistry for Alternative Energy Sources and Environmental Improvement*; Palomar-Pardave, M., Romero-Romo, M., Montiehsantillan, T., Gonzalez, I., Duron-Torres, S. M., Escalante-Garcia, I. L., Eds.; Electrochemical Society: Pennington, NJ, **2010**; Chapter 1, p 1.
56. Quraishi, M. A.; Ansar, K. R.; Ebenso, E. E. *Int. J. Electrochem. Sci.* **2012**, *7*, 13106.
57. Bribri, A. E.; Tabyaoui, M.; Tabyaoui, B.; Attari, H. E.; Bentiss, F. *Mater. Chem. Phys.* **2013**, *141*, 240.
58. Etaiwa, S. E. H.; Foudab, A. E. S.; Elbendarya, M. M. *Prot. Met. Phys. Chem. Surf.* **2013**, *49*, 113.
59. Patil, S.; Sainkar, S. R.; Patil, P. P. *Appl. Surf. Sci.* **2004**, *225*, 204.
60. Kumar, S. A.; Meenakshi, K. S.; Sankaranarayanan, T. S. N.; Srikanth, S. *Prog. Org. Coat.* **2008**, *62*, 285.
61. Opdahl, A.; Koffas, T. S.; Amitay-Sadovsky, E.; Kim, J.; Somorjai, G. A. *J. Phys. Condens. Matter* **2004**, *16*, 659.
62. Löberg, J.; Mattisson, I.; Hansson, S.; Ahlberg, E. *Open Biomater. J.* **2010**, *2*, 18.
63. Arslan, T.; Kandemirli, F.; Ebenso, E. E.; Love, I.; Alemu, H. *Corros. Sci.* **2009**, *51*, 35.
64. Ebenso, E. E.; Isabirye, D. A.; Eddy, N. O. *Int. J. Mol. Sci.* **2010**, *11*, 2473.
65. Li, X.; Deng, S.; Fu, H.; Li, T. *Electrochim. Acta* **2009**, *54*, 4089.
66. Al-Sabagh, A. M.; Nasser, N. M.; Farag, A. A.; Migahed, M. A.; Eissa, A. M. F.; Mahmoud, T. *Egypt J. Pet.* **2013**, *22*, 101.